Facile synthesis of Fe_3O_4/g-C_3N_4/HKUST-1 composites as a novel biosensor platform for ochratoxin A

Shuisheng Hu, Wenjun Ouyang, Longhua Guo, Zhenyu Lin, Xiaohua Jiang, Bin Qiu, Guonan Chen

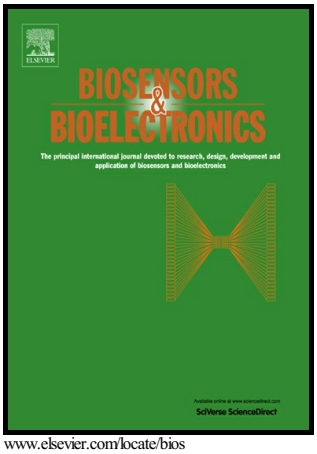

www.elsevier.com/locate/bios

PII: S0956-5663(16)30996-4
DOI: http://dx.doi.org/10.1016/j.bios.2016.10.006
Reference: BIOS9227

To appear in: *Biosensors and Bioelectronic*

Received date: 24 July 2016
Revised date: 27 September 2016
Accepted date: 1 October 2016

Cite this article as: Shuisheng Hu, Wenjun Ouyang, Longhua Guo, Zhenyu Lin Xiaohua Jiang, Bin Qiu and Guonan Chen, Facile synthesis of Fe_3O_4/g C_3N_4/HKUST-1 composites as a novel biosensor platform for ochratoxin A *Biosensors and Bioelectronic,* http://dx.doi.org/10.1016/j.bios.2016.10.006

Facile synthesis of Fe_3O_4/g-C_3N_4/HKUST-1 composites as a novel biosensor platform for ochratoxin A

Shuisheng Hu[a], Wenjun Ouyang[a], Longhua Guo[a], Zhenyu Lin[a,b], Xiaohua Jiang[c*], Bin Qiu[a1*],Guonan Chen[a]

[a]Ministry of Education Key Laboratory of Analysis and Detection for Food Safety, Fujian Provincial Key Laboratory of Analysis and Detection for Food Safety, Fuzhou University, Fuzhou, Fujian, 350108, P. R. China

[b]State Key Laboratory of Photocatalysis on Energy and Environment, College of Chemistry, Fuzhou University, Fuzhou 350002, P. R. China

[c]School of Applied Chemistry and Biological Technology, Shen zhen Polytechnic, Shenzhen, Guangdong, 518055, P. R. China

summer328cn@163.com (Bin Qiu)

remotexh@ustc.edu.cn (Xiaohua Jiang)

[*]Corresponding author. Department of Chemistry, Fuzhou University, Fuzhou, Fujian, 350108, China.

[1] Tel & Fax: 86-591-22866135

Abstract

A fluorescent biosensor for ochratoxin A was fabricated on the basis of a new nanocomposite (Fe_3O_4/g-C_3N_4/HKUST-1 composites). Fe_3O_4/g-C_3N_4/HKUST-1 was synthesized in this work for the first time, which combined HKUST-1 with g-C_3N_4 to improve its chemical stability. Fe_3O_4/g-C_3N_4/HKUST-1 composites have strong adsorption capacity for dye-labeled aptamer and are able to completely quench the fluorescence of the dye through the photoinduced electron transfer (PET) mechanism. In the presence of ochratoxin A (OTA), it can bind with the aptamer with high affinity, causing the releasing of the dye-labeled aptamer from the Fe_3O_4/g-C_3N_4/HKUST-1 and therefore results in the recovery of fluorescence. The fluorescence intensity of the biosensor has a linear relationship with the OTA concentration in the range of 5.0－160.0 ng/mL. The LOD of sensor is 2.57 ng/mL (S/N = 3). This fluorescence sensor based on the Fe_3O_4/g-C_3N_4/HKUST-1 composites has been applied to detect OTA in corn with satisfying results.

Keywords: Fe_3O_4/g-C_3N_4/HKUST-1 composites; ochratoxin A; aptamer; fluorescent biosensor

1. Introduction

Metal-organic frameworks (MOFs), crystalline molecular materials, have been

broadly used in various applications, such as adsorption(Xiao et al. 2016), separation(Zhang et al. 2016), catalysis(Corma et al. 2010), sensing(Hu et al. 2014), and drug delivery(Horcajada et al. 2010), owing to their unique physical and chemical properties (e.g., unprecedentedly large surface area and permanent inner porosity). Most of the work aims at designing new kinds of MOFs and exploring their corresponding applications. Nevertheless, MOFs present some drawbacks such as poor chemical stability (Decoste et al. 2012; Hao and Yan 2015), hindering their potential application, especially the practical application. To meet the practical application, it is prerequisite to address this issue and is desirable to further search their potential property and new functionality.

Combining MOFs with other superior functional materials has attracted increasing attention because this protocol may take advantage of their merits and mitigate their shortcomings (Falcaro et al. 2011; Khaletskaya et al. 2013). To date, many investigations have been reported on the combination of MOFs with active species, including quantum dots (QDs)(Saha et al. 2014), polyoxometalates (POMs)(Sun et al. 2009), polymers(Uemura et al. 2009), grapheme (Li et al. 2014), and carbon nanotubes (CNTs)(Wang et al. 2013). Other fascinating nanomaterials like two-dimensional (2D) layered materials have also gained increasing attention for their distinct biocompatible, electronic, optical, and adsorptive properties(Chhowalla et al. 2013). Of these

2D nanomaterials, graphitic-phase carbon nitride (g-C_3N_4), an analogue of graphite, possesses a stacked 2D structure; it can be regarded as N-substituted graphite in a regular fashion(Thomas et al. 2008). g-C_3N_4 has been extensively applied in sensing(Cheng et al. 2013), drug delivery(Lin et al. 2014), imaging(Zhang et al. 2014a), and environmental applications(Ma et al. 2014) owing to its unique features. However, g-C_3N_4 possesses intrinsic shortcomings such as low affinity of aptamer and small molecules, which may result in the easy desorption of aptamer from the surface of the material without the addition of target molecule and hence may decrease the stability of sensor (Ping et al. 2015). Consequently, in this report one strategy being referenced that combines HKUST-1 (HKUST-1 is chosen as a kind of classical metal organic framework) with g-C_3N_4, also acting as a hydrophobic "shield" to prevent the open metal sites of HKUST-1 from being occupied by water molecules, which is similar to the combination of MOF with carbone nanotube(Zhang et al. 2014). To the best of our knowledge, no work has been reported on g-C_3N_4/HKUST-1 composite.

Ochratoxin A (OTA), a type of mycotoxin, has been reported as one of the most toxic and cancerigenic substances to a wide variety of mammalian species(Duarte et al. 2010b). Besides, OTA can pollute a series of food, including cereals, wheat, barley, beans, corn, coffee, and wine, and causing a threat to human health(Duarte et al. 2010a). Note that the contamination from OTA in food samples does not cause any observable physical damage (decay,

mildew, etc.) in the early stage of infection. Thus it is hard to diagnose OTA in the initial infection stage(McKeague et al. 2014). Many colorimetric, electrochemical, fluorescent, and surface plasmon resonance biosensors have been proposed for the detection of low concentration of OTA (Lee et al. 2014; Rivas et al. 2015; Wang et al. 2015; Zhu et al. 2015). However, these methods have some disadvantages, such as complicated operation, time-consuming process, and poor specificity. To avoid further deteriorate, it is still necessary to propose a novel method for detection of probably low level of OTA.

Herein, the as-synthesized g-C_3N_4/HKUST-1 composite was employ to develop biosensor for the detection of OTA for the first time. To lower the background, Fe_3O_4 was also introduced to the as-synthesized composite to form Fe_3O_4/g-C_3N_4/HKUST-1. The as-synthesized Fe_3O_4/g-C_3N_4/HKUST-1 was characterized using transmission electron microscopy (TEM), X-ray diffraction (XRD), Brunner-Emmet-Teller (BET), and Fourier transform infrared spectroscopy (FTIR). This proposed strategy was eventually adopted to detect OTA in corn samples. Such protocol may open the door for the application of Fe_3O_4/g-C_3N_4/HKUST-1 in fluorescence analysis.

2. Experimental section

2.1 Reagents and instruments

All nucleotide sequences were synthesized and purified by the Biological Engineering Technology Service Co. (Shanghai, China). Copper nitrate

trihydrate, anhydrous alcohol, and 1, 3, 5-benzenetricarboxylic acid (trimesic acid, H_3BTC) were obtained from Aladdin (Shanghai, China). Dicyandiamide, Ochratoxin A (OTA), Ochratoxin B (OTB), Ochratoxin C (OTC), Aflatoxin B1 (AFB1) and Zearalenone (ZEN) were supplied by Sigma Aldrich (USA). All chemicals used were of analytical grade. The quality control corn samples were purchased from Clover Technology Group, Inc. (Beijing, China). Deionized water was from a Milli-Q water purification system (Millipore, USA,18.2 MΩ·cm).

OTA aptamer sequence: 5'-FAM-GAT CGG GTG TGG GTG GCG TAA AGG GAG CAT CGG ACA-3'

Fluorescence spectra were recorded on an F-4600 fluorescence spectrophotometer (HITACHI, Japan) equipped with a Xenon lamp. The fluorescence emission spectra were recorded at the excitation and emission wavelengths of 480 and 520 nm, respectively.

2.2 Synthesis of g-C_3N_4 nanosheets

Bulk g-C_3N_4 was prepared as previously reported(Yan et al. 2009). Briefly, dicyandiamide was heated from room temperature to 550 ℃ with a ramp rate of 2.3 ℃/min under static air, and then the temperature was kept at 550 ℃ for 4 h. To protonate the resulting bulk g-C_3N_4, 0.3 g of the obtained material was dispersed in 200 mL of deionized water, followed by sonication-exfoliation for

6 h. The mixture was centrifuged at 3000 rpm to remove unexfoliated aggregates, g-C_3N_4 nanosheets (g-C_3N_4 NS) were finally obtained. The supernatant was concentrated at 60 ℃ until the volume of solution was about 50 mL.

2.3 Synthesis of Fe_3O_4 particles

The spherical Fe_3O_4 particles were prepared according to the literature(Liu et al. 2009), but with some modification. $FeCl_3 \cdot 6H_2O$ (6.5 g) and tri-sodium citrate (2.0 g) were dissolved in ethylene glycol solution (120 mL) through ultrasound irradiation, followed by adding sodium acetate (12 g) under vigorous stirring for 15 min. The resultant mixture was then transferred to a 150 mL Teflon-lined stainless-steel autoclave for heating at 200 ℃ for 8 h. After that, the autoclave was carefully taken out and cooled down to room temperature. The as-prepared black products were thoroughly washed with ethanol and deionized water three times, respectively, and dried in a vacuum oven before using.

2.4 Synthesis of Fe_3O_4/g-C_3N_4/HKUST-1

The Fe_3O_4/g-C_3N_4/HKUST-1 was synthesized by a solvothermal reaction. Briefly, $Cu(NO_3)_2 \cdot 3H_2O$ (1.087 g, 4.5 mM) was firstly dissolved in 15 mL of water containing 10 mL of g-C_3N_4 NS and then mixed with 0.525 g of H_3BTC (2.5 mM) which was dissolved in 15 mL of ethanol. The mixture was stirred for 30 min, followed by adding Fe_3O_4 (0.3 g). The final mixture was transferred to

a Teflon autoclave liner and sealed for heating at 120 ℃ for 12 h. The obtained light blue powder was filtered, washed several times with water and ethanol, and then dried overnight at 100 ℃ under vacuum condition.

2.5 Characterization

TEM images were obtained with a FEI Tecnai G2 F20 (FEI, USA). XRD was determined using a D8 Advance (Bruker, German). The surface area and pore diameter were determined with a physisorption analyzer (Micromeritics ASAP 2020 porosimeter, USA). BET was performed to calculate the specic surface areas using adsorption data at p/p_0 of 0.05−0.3. The total pore volume (V_t) was estimated from the adsorbed amount at p/p_0 of 0.995. FTIR was conducted using a FTIR spectrophotometer (Nicolet 6700, Waltham, MA, USA).

2.6 Detection of OTA

FAM-labelled aptamer (50 nM) was prepared in Tris-HCl buffer (50 mM, pH 7.4), and mixed with Fe_3O_4/g-C_3N_4/HKUST-1 for 30 min. Use magnet to separate aptamer haven not loaded in Fe_3O_4/g-C_3N_4/HKUST-1, then added buffer to redispersed the aptamer loaded Fe_3O_4/g-C_3N_4/HKUST-1. Different concentrations of OTA were subsequently added to the mixed solution and incubation for 60 min at room temperature. Magnet was used to separate the supernate and Fe_3O_4/g-C_3N_4/HKUST-1. Fluorescence signal was finally obtained from supernatant.

3. Results and Discussion

3.1 Characterization

Fig. 1 shows the TEM images of the as-synthesized materials including Fe_3O_4, g-C_3N_4, HKUST-1, and Fe_3O_4/g-C_3N_4/HKUST-1. Fig. 1A clearly shows that the Fe_3O_4 particles were quasi-spherical with a diameter of about 200 nm. The morphology of g-C_3N_4 NS is shown in Fig. 1B, where a size of 1.5 μm was observed. Fig. 1C reveals that the HKUST-1 was octahedron with a diameter of about 1 μm. Unlike the perfect crystalline HKUST-1, Fe_3O_4/g-C_3N_4/HKUST-1 shows a distorted structure which is possibly assembled by bridging g-C_3N_4 NS and Fe_3O_4 to the surface of MOFs porous network (Fig. 1D), possibly suggesting the successful synthesis of Fe_3O_4/g-C_3N_4/HKUST-1.

Fig. S1A shows the XRD patterns of Fe_3O_4, g-C_3N_4, HKUST-1, and Fe_3O_4/g-C_3N_4/HKUST-1. Line a in Fig. S1A reveals the existence of the characteristic signal at 2θ of 30.3°, 35.7°, and 43.3° marked by their indices (220), (311), (400), respectively, indicating the crystalline in nature (JCPDS file 19-0629)(Zeng et al. 2013b). For g-C_3N_4 (line b, Fig. S1A), the strong shoulder peak at 2θ of 27.4° (d = 0.326 nm) and the low-angle diffraction peak at 2θ of 13.3° (d = 0.663 nm) originated from the (002) interlayer diffraction of a CN

graphitic-like structure and inplanar repeated tris-triazine units, respectively. The diffraction peaks of HKUST-1 matched well with those in previous report (line c, Fig. S1A) (Ke et al. 2011), in which HKUST-1 was well crystallized. The XRD pattern of Fe_3O_4/g-C_3N_4/HKUST-1 was similar to that of HKUST-1, suggesting that the structure of HKUST-1 is also crystalline.

Fig. S1B and S1C present the porous properties of Fe_3O_4, g-C_3N_4, HKUST-1, and Fe_3O_4/g-C_3N_4/HKUST-1, and Table S1 lists their corresponding BET surface area and total pore volume. Compared with the HKUST-1 (1188.7373 m^2/ g, 0.6483 cm^3/g),the resulting Fe_3O_4/g-C_3N_4/HKUST-1 displayed no significant variations; there was slight decrease of BET surface area (952.9173 m^2/g) and gradual increase of total pore volume (1.02907 cm^3/g).

Fig. S1 presents the FTIR spectra of Fe_3O_4, g-C_3N_4, HKUST-1, and Fe_3O_4/g-C_3N_4/HKUST-1. In curve a, the peaks at 1637 and 1243 cm^{-1} are attributable to the C=N and C-N stretching vibration modes, respectively(Zhao et al. 2005). The peak at 808 cm^{-1} is related to the s-triazine ring modes(Li et al. 2009). In curve b, peak observed at 585 cm^{-1} is due to the Fe-O vibration. The adsorption peak at 1400 cm^{-1} is for the vibration of COO^- group from citrate on the surface of Fe_3O_4, and the broad peak at 1626 cm^{-1} corresponds to the vibration of overlapping COO^- and H-O groups(Zeng et al. 2013a). The Fe-O vibration was observed in both spectra for Fe_3O_4 and Fe_3O_4/g-C_3N_4/HKUST-1, but the intensity of this peak for

Fe_3O_4/g-C_3N_4/HKUST-1 decreased probably because of the immobilization of the coated HKUST-1. In curve c, the asymmetric stretching of carboxylate group in H_3BTC appeared at 1508−1623 cm^{-1}, and the symmetric stretching of the carboxylate groups in H_3BTC was observed at 1384 and 1405 cm^{-1}. Several bands observed in the region of 1300−600 cm^{-1} are assigned to the out-of-plane vibrations of H_3BTC. All abovementioned characteristic peaks appeared in the spectra for Fe_3O_4/g-C_3N_4/HKUST-1 (curve d), suggesting the successful synthesis of Fe_3O_4/g-C_3N_4/HKUST-1.

3.2 Principle of the proposed fluorescence sensor

As shown in Scheme 1, Fe_3O_4/g-C_3N_4/HKUST-1 was firstly synthesized. It has strong adsorption capacity for dye-labeled aptamer and then completely quenches the fluorescence of the dye(Marras et al. 2002). In the presence of OTA, the binding interaction between the dye-labeled aptamer and OTA is higher than that between the dye-labeled aptamer and Fe_3O_4/g-C_3N_4/HKUST-1, leading to the releasing of the dye-labeled aptamer from the Fe_3O_4/g-C_3N_4/HKUST-1 and therefore results in the recovery of fluorescence. Herein, the magnet was used to separate the Fe_3O_4/g-C_3N_4/HKUST-1 and solution. This proposed design can be adopted for the determination of OTA through a fluorescence enhanced platform.

3.3 Feasibility of the proposed fluorescence sensor

To validate the feasibility of this strategy, consecutive study was carried out, and Fig. 2 presents the corresponding fluorescence intensity (FL intensity). Previous studies have indicated that the aptamer binds with MOF through hydrogen bonding interaction(Wei et al. 2013) and aptamer binds with g-C_3N_4 through hydrogen bonding interaction and π-stacking(Wang. et al. 2009), so we speculate that the aptamer binds with Fe_3O_4/g-C_3N_4/HKUST-1 in this study may via hydrogen bonding interaction and π-stacking. Upon the addition of Fe_3O_4/g-C_3N_4/HKUST-1 to the FAM-labeled ssDNA solution, the FL intensity dramatically decreased (curve a to b), and the quench effect (QE) was approx. 87.23%. Moreover, the FL intensity reached the plateau within 30 min (As shown in Fig. S2B), indicating the fast quenching kinetics of Fe_3O_4/g-C_3N_4/HKUST-1. The reason why significantly decrease of FL intensity was observed is probably due to the electronic communication between the photoexcited electrons from fluorophore to the conductive band of Fe_3O_4/g-C_3N_4/HKUST-1 through the photoinduced electron transfer (PET) mechanism. The FL intensity remarkably recovered upon the addition of different concentrations of OTA to the solution (line c to e); the recovery efficiency increased as the concentration rose.

Furthermore, the role of HKUST-1 and Fe_3O_4 in Fe_3O_4/g-C_3N_4/HKUST-1 has been investigated. In order to compare the influence of MOF in composite, g-C3N4 and Fe_3O_4/HKUST-1/g-C_3N_4 was used to quench the fluorescence of day labbled-aptamer. As shown in Fig. S2A, the result shows that with MOF, the material could easy quench the fluorescence of FAM than g-C_3N_4. The Fe_3O_4 was introduced to the as-synthesized composite to form Fe_3O_4/g-C_3N_4/HKUST-1 to reduce the background of the sensors. As shown in Fig. S2B, the fluorescence of FAM-labbled aptamer was quenched by Fe_3O_4/g-C_3N_4/HKUST-1, we compared the fluorescence intensity of separate by magnet and without separate. The results demonstrate that the background of the sensors could be reduced with magnet separate. Hence, Fe_3O_4/g-C_3N_4/HKUST-1 can be used as the sensing platform for OTA detection.

3.4 Optimization of experimental conditions

The parameters which affect the performance of the biosensor were optimized. Fig. S3A displays the effect of the dosage of Fe_3O_4/g-C_3N_4/HKUST-1, as the dosage of Fe_3O_4/g-C_3N_4/HKUST-1 increased, the FL intensity declined obviously and reached a plateau at round 30 μL. Therefore, the dosage of Fe_3O_4/g-C_3N_4/HKUST-1 was selected at 30 μL. Reaction time for quenching and recover was optimized separately. Fig. S3B shows FL intensity decreased with the extension of time and reached a plateau after 30 min, whereas FL intensity recovered as the time increased and reached stable at around 60 min (Fig. S3C). Hence 30 min and 60 min were chosen as the quenching and recovery time, respectively.

3.5 Quantitative detection of OTA

Fig. 3A shows the typical FL intensity with different concentrations of OTA under the optimized conditions, where the FL intensity gradually increased with the increment of OTA concentration in the range of 5.0 to 160 ng/mL. Fig. 3B presents the relationship between the enhanced FL intensity (ΔF, the difference intensity between the presence and absence of OTA). There was a linear relationship between ΔF and the concentration of OTA with a correlation coefficient of 0.992. The linear equation was $\Delta F = 1.697 + 1.058\ C_{OTA}$. The detection limit was 2.57 ng/mL (S/N = 3).

3.6 Selectivity and repeatability of biosensor

The selectivity of the proposed biosensor was also evaluated. The concentrations of the interferents including OTB, OTC, AFB1, and ZEN were 100-fold of the OTA (160 ng/mL). The FL intensity for OTB, OTC, AFB1, and ZEN showed no obvious variation, whereas OTA induced great recovery (Fig. 4). These results indicate that the proposed biosensor has good selectivity to target. To estimate the repeatability, we repeated the assay six times using the proposed biosensor under the optimized conditions. The relative standard deviation (RSD) was 2.5%, indicating a good repeatability.

3.7 Determination of OTA in corn samples

The practicality of the proposed fluosensor was verified by measuring OTA in the corn samples. The quality control corn samples were purchased from Clover Technology Group, Inc. (Beijing, China) with reference concentration of OTA in 162.60 ppb (162.60 ng/g). Corn samples (4.0 g) were firstly extracted by 20.0 mL of 80% methanol solution, and then stirred overnight. OTA solution was finally filtered, and the concentration was 32.52 ng/mL (equivalent to162.60 ng/g). The obtained OTA solution was performed by proposed method, the concentrations of OTA in corn samples were 31.87, 33.45, 32.14 ng/mL, which are equivalent to 159.36, 167.28, and 160.71 ng/g, respectively. The recovery rates were 200.00, 400.00, and 600.00 ng/g, respectively. OTA standard solutions were eventually spiked to the above mentioned samples. As shown in Table 1, the recovery rates were in the range of 96.5–101.4%. These results demonstrate the practical application of the proposed method. Compared with most developed approaches for OTA detection, the analytical figure of merit of the proposed method is also superior (shown in Table 2).

4. Conclusion

In summary, a facile and rapid biosensor has been engineered for the detection of OTA based on the Fe_3O_4/g-C_3N_4/HKUST-1 composites for the first time. Experimental results have demonstrated such biosensor possesses high sensitivity and selectivity. More importantly, this biosensor has been successfully applied to detect OTA in the corn samples with satisfied results. This strategy may have a promising prospect for target detection in food analysis.

Acknowledgements

The authors gratefully acknowledge the financial support of the National Natural Science Foundation of China (21375021), Key Project of Fujian Province (2015Y0050). Nature Sciences Funding of Fujian Province(2014J06005) and the Independent Research Project of State Key Laboratory of Photocatalysis on Energy and Environment (NO. 2014B02).

References

Bazin, I., Andreotti, N., Hassine, A.I., De Waard, M., Sabatier, J.M., Gonzalez, C., 2013. Biosens. Bioelectron. 40(1), 240-246.

Cheng, C., Huang, Y., Wang, J., Zheng, B., Yuan, H., Xiao, D., 2013. Anal. Chem 85(5), 2601-2605.

Chhowalla, M., Shin, H.S., Eda, G., Li, L.-J., Loh, K.P., Zhang, H., 2013. Nat. Chem 5(4), 263-275.

Corma, A., García, H., Llabrés i Xamena, F., 2010. Chem. Rev 110(8), 4606-4655.
Decoste, J.B., Peterson, G.W., Smith, M.W., Stone, C.A., Willis, C.R., 2012. J Am Chem Soc 134(3), 1486-1489.
Duarte, S., Lino, C., Pena, A., 2010a. Food Addit. Contam., Part A 27(10), 1440-1450.
Duarte, S., Pena, A., Lino, C., 2010b. Food. Microbiol 27(2), 187-198.
Falcaro, P., Hill, A.J., Nairn, K.M., Jasieniak, J., Mardel, J.I., Bastow, T.J., Mayo, S.C., Gimona, M., Gomez, D., Whitfield, H.J., 2011. Nat. Commun 2, 237.
Guo, Z., Ren, J., Wang, J., Wang, E., 2011. Talanta 85(5), 2517-2521.
Hao, J.N., Yan, B., 2015. Chem. Commun. 51(36), 7737-7740.
Horcajada, P., Chalati, T., Serre, C., Gillet, B., Sebrie, C., Baati, T., Eubank, J.F., Heurtaux, D., Clayette, P., Kreuz, C., 2010. Nat.Mater 9(2), 172-178.
Hu, Z., Deibert, B.J., Li, J., 2014. Chem. Soc. Rev 43(16), 5815-5840.
Ke, F., Yuan, Y.-P., Qiu, L.-G., Shen, Y.-H., Xie, A.-J., Zhu, J.-F., Tian, X.-Y., Zhang, L.-D., 2011. J. Mater. Chem 21(11), 3843-3848.
Khaletskaya, K., Reboul, J., Meilikhov, M., Nakahama, M., Diring, S.p., Tsujimoto, M., Isoda, S., Kim, F., Kamei, K.-i., Fischer, R.A., 2013. J. Am. Chem. Soc 135(30), 10998-11005.
Lee, J., Jeon, C.H., Ahn, S.J., Ha, T.H., 2014. Analyst 139(7), 1622-1627.
Li, Q., Xu, P., Gao, W., Ma, S., Zhang, G., Cao, R., Cho, J., Wang, H.L., Wu, G., 2014. Adv. Mater 26(9), 1378-1386.
Li, X., Zhang, J., Shen, L., Ma, Y., Lei, W., Cui, Q., Zou, G., 2009. Appl. Phys. A: Mater. Sci. Process 94(2), 387-392.
Lin, L.-S., Cong, Z.-X., Li, J., Ke, K.-M., Guo, S.-S., Yang, H.-H., Chen, G.-N., 2014. J. Mater. Chem. B 2(8), 1031-1037.
Liu, J., Sun, Z., Deng, Y., Zou, Y., Li, C., Guo, X., Xiong, L., Gao, Y., Li, F., Zhao, D., 2009. Angew. Chem 121(32), 5989-5993.
Liu., B.H., Tsao., Z.J., Wang., J.J., Yu., F.Y., 2008. Anal. Chem 80, 7029-7035.
Ma, T.Y., Dai, S., Jaroniec, M., Qiao, S.Z., 2014. Angew. Chem., Int. Ed 53(28), 7281-7285.
Marras, S.A., Kramer, F.R., Tyagi, S., 2002. Nucleic Acids Res 30(21), e122-e122.
McKeague, M., Velu, R., Hill, K., Bardóczy, V., Mészáros, T., DeRosa, M.C., 2014. Toxins 6(8), 2435-2452.
Ping, J., Zhou, Y., Wu, Y., Papper, V., Boujday, S., Marks, R.S., Steele, T.W., 2015. Biosens. Bioelectron. 64, 373-385.
Rivas, L., Mayorga-Martinez, C.C., Quesada-González, D., Zamora-Gálvez, A., de la Escosura-Muñiz, A., Merkoçi, A., 2015. Anal. Chem 87(10), 5167-5172.
Saha, S., Das, G., Thote, J., Banerjee, R., 2014. J. Am. Chem. Soc 136(42), 14845-14851.
Sheng, L., Ren, J., Miao, Y., Wang, J., Wang, E., 2011. Biosens. Bioelectron. 26(8), 3494-3499.
Sun, C.-Y., Liu, S.-X., Liang, D.-D., Shao, K.-Z., Ren, Y.-H., Su, Z.-M., 2009. J. Am. Chem. Soc 131(5), 1883-1888.
Thomas, A., Fischer, A., Goettmann, F., Antonietti, M., Müller, J.-O., Schlögl, R., Carlsson, J.M., 2008. J. Mater. Chem 18(41), 4893-4908.
Uemura, T., Yanai, N., Kitagawa, S., 2009. Chem. Soc. Rev 38(5), 1228-1236.
Wang, C., Qian, J., Wang, K., Wang, K., Liu, Q., Dong, X., Wang, C., Huang, X., 2015. Biosens. Bioelectron 68, 783-790.
Wang, Y., Wu, Y., Xie, J., Ge, H., Hu, X., 2013. Analyst 138(17), 5113-5120.

Wang., Y., Shi., Z., Huang., Y., Ma., Y., Wang., C., Chen., M., Chen., Y., 2009. J. Phys. Chem. C 113, 13103–13107.

Wei, X., Zheng, L., Luo, F., Lin, Z., Guo, L., Qiu, B., Chen, G., 2013. J. Mater. Chem. B 1(13), 1812.

Xiao, D.J., Gonzalez, M.I., Darago, L.E., Vogiatzis, K.D., Haldoupis, E., Gagliardi, L., Long, J.R., 2016. J. Am. Chem. Soc.

Yan, S., Li, Z., Zou, Z., 2009. Langmuir 25(17), 10397-10401.

Yang, C., Wang, Y., Marty, J.L., Yang, X., 2011. Biosens. Bioelectron. 26(5), 2724-2727.

Zeng, T., Niu, H.-y., Ma, Y.-r., Li, W.-h., Cai, Y.-q., 2013a. Appl. Catal., B 134, 26-33.

Zeng, T., Zhang, X., Ma, Y., Wang, S., Niu, H., Cai, Y., 2013b. Chem. Commun 49(54), 6039-6041.

Zhang, W., Banerjee, D., Liu, J., Schaef, H.T., Crum, J.V., Fernandez, C.A., Kukkadapu, R.K., Nie, Z., Nune, S.K., Motkuri, R.K., 2016. Adv. Mater.

Zhang, X., Wang, H., Wang, H., Zhang, Q., Xie, J., Tian, Y., Wang, J., Xie, Y., 2014. Adv. Mater 26(26), 4438-4443.

Zhang, Z., Huang, Y., Ding, W., Li, G., 2014. Anal chem. 86(7), 3533-3540.

Zhao, Y., Yu, D., Zhou, H., Tian, Y., Yanagisawa, O., 2005. J. Phys. Chem. B 40(9), 2645-2647.

Zhu, Z., Feng, M., Zuo, L., Zhu, Z., Wang, F., Chen, L., Li, J., Shan, G., Luo, S.-Z., 2015. Biosens. Bioelectron 65, 320-326.

Scheme 1 The principle of the biosensor based on Fe_3O_4/g-C_3N_4/HKUST-1 to detect OTA

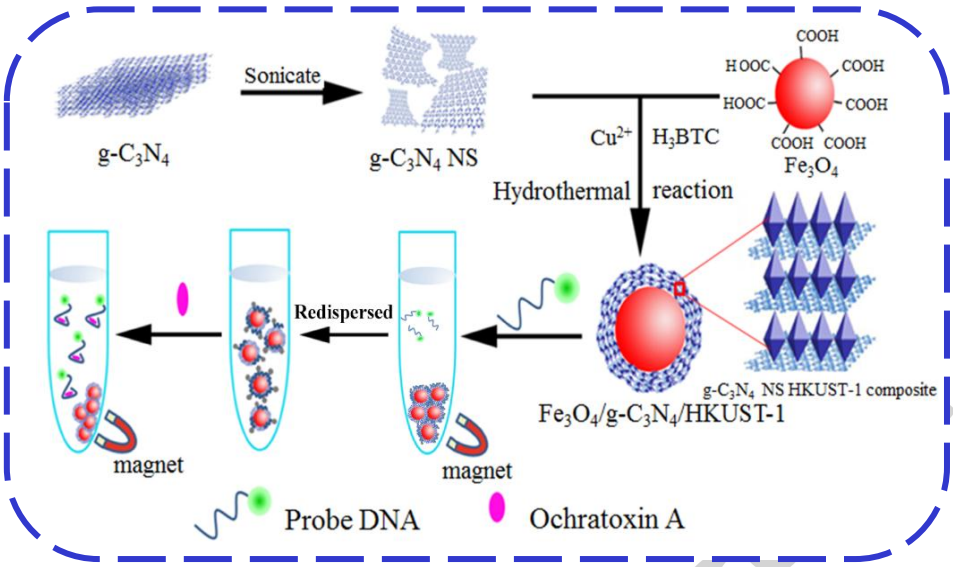

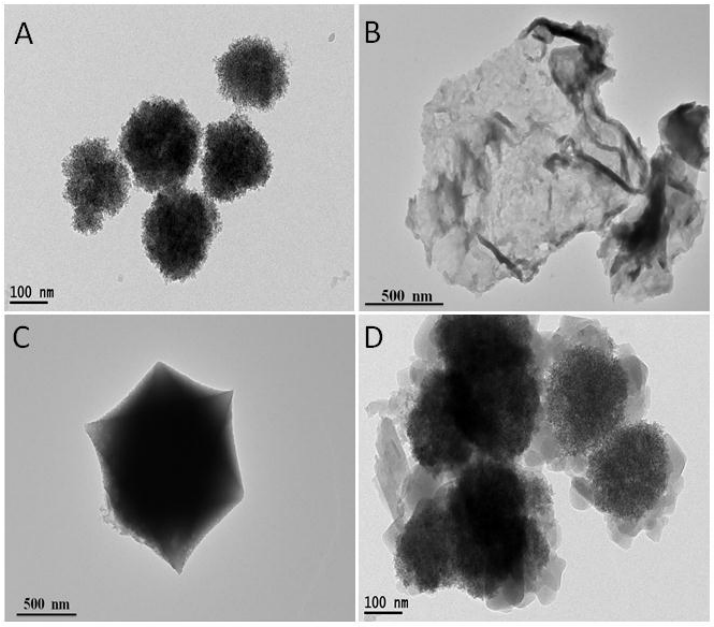

Fig. 1 TEM images for synthesis materials, TEM images for (A) Fe_3O_4, (B) g-C_3N_4, (C) HKUST-1, (D) Fe_3O_4/g-C_3N_4/HKUST-1

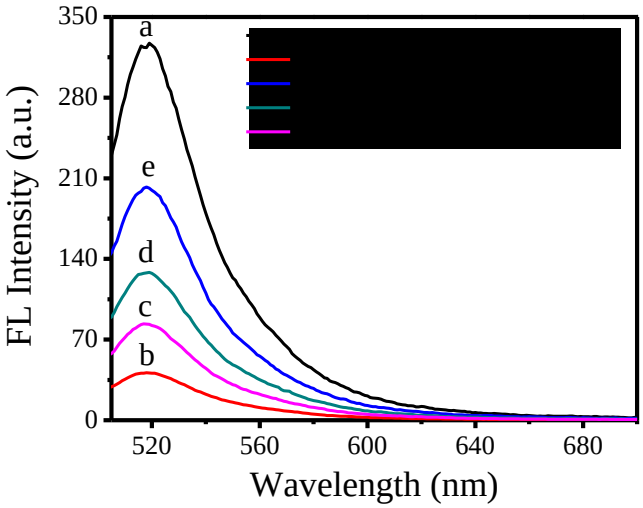

Fig. 2 Fluorescence spectra of assistant test to verify principle, FL intensity in the presence of (a) aptamer; (b) aptamer + Fe_3O_4/g-C_3N_4/HKUST-1 (50 μL); (c) b + 40 ng/mL OTA; (d) b + 80 ng/mL OTA (e) b + 160 ng/mL OTA

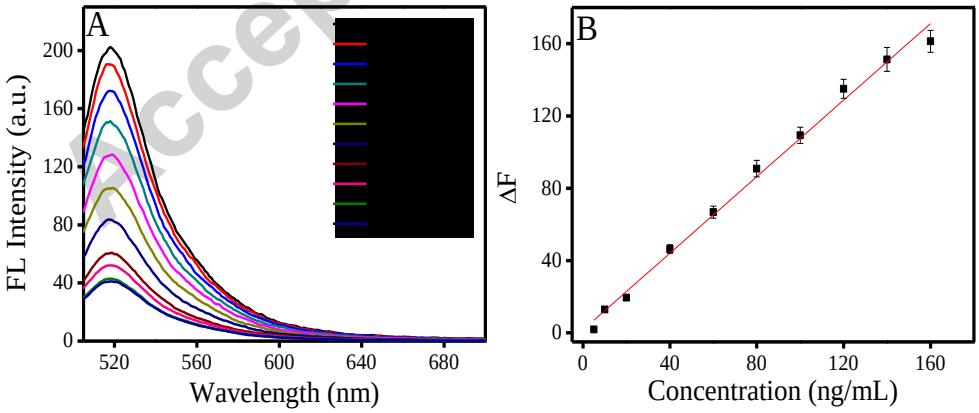

Fig. 3 Quantitative assays of the OTA, (A) Fluorescence spectra with varying concentrations of OTA; (B) The relationship between ΔF and the OTA concentration, OTA-aptamer (50 nM), Fe_3O_4/g-C_3N_4/HKUST-1 (30 μL, 50 μg/mL).

Fig. 4 Selectivity of the proposed biosensor

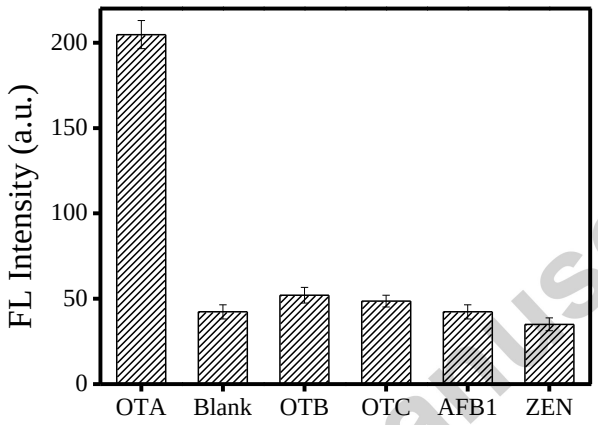

Table. 1 Determination of OTA in corn samples

Sample	Detected (ng/g)	Reference (ng/g)	Spiked (ng/g)	Total found (ng/g)	Recovery	RSD
1	159.36	162.60	200.00	352.36	96.5%	5.2%
2	167.28	162.60	400.00	570.88	100.9%	4.5%
3	160.71	162.60	600.00	769.11	101.4%	5.6%

Table.2 Comparison with currently established/accepted methods for OTA detection

Method	Dynamic range	LOD of OTA	Ref
ELISA	0-100.0 ng/mL	5.0 ng/mL	(Liu. et al. 2008)
HPLC-FLD	1.25-10.0 ng/mL	1.25 ng/mL	(Bazin et al. 2013)
PVP-coated graphene oxide	2.0-35.0 μM	1.9 μM	(Sheng et al. 2011)
AuNPs.	20.0-625.0 nM	20.0 nM	(Yang et al. 2011)
single-walled carbon nanotubes (SWNTs)	25.0-200.0 nM	24.1 nM	(Guo et al. 2011)
Fe_3O_4/g-C_3N_4/HKUST-1	5.0 - 160.0 ng/mL	2.57 ng/mL	This Work

Highlights

- Combining metal-organic frameworks with Graphitic carbon nitride can mitigate the shortcomings of MOFs.
- A fluorescence biosensor for ochratoxin A was fabricated based on Fe_3O_4/g-C_3N_4/HKUST-1 composites.
- Aptamer has high specificity and flexibility for target.